ARTICLE OPEN

Check for updates

Stress granules promote DNA damage repair through the *G3BP1/NAT10/ATF3* axis to facilitate nasopharyngeal carcinoma progression

Tian Yue[1,5], Haimeng Yin[2,3,5], Ling Yuan[2,3,5], Xincheng Xie[2,3], Haijing Xie[2,3], Mengfang Gong[1], Xian Xu[1], Chunxiao Sun[4], Kaiwen Zhang[2,3]✉ and Jisheng Liu[1]✉

Aberrantly enhanced DNA damage repair contributes to therapy resistance and poor prognosis in nasopharyngeal carcinoma (NPC), but its regulatory mechanisms remain unclear. Stress granules (SGs) mediate tumor stress adaptation, yet their role in NPC DNA damage repair is unknown. Here, we show that SGs are significantly enriched in NPC cells under stress, and the SG core protein G3BP1 is highly expressed in NPC tissues ($n = 111$), correlating with metastasis and poor survival. Mechanistically, under stress, N-acetyltransferase 10 (NAT10)-catalyzed N4-acetylcytosine (ac4C) modification targets mRNAs of DNA repair genes (*ATF3, LIG1, RNF168*) to SGs, protecting them from degradation. Upon stress relief, these mRNAs are released for translation, enhancing DNA damage repair. The *G3BP1/NAT10/ATF3* axis is critical for NPC DNA repair and metastasis, as blocking this axis (via *G3BP1* depletion, NAT10 inhibitor remodelin, or *ATF3* knockout) inhibits tumor growth and metastasis in vitro and in vivo. This study uncovers a novel ac4C-dependent mechanism by which SGs regulate DNA damage repair in NPC, identifying the *G3BP1/NAT10/ATF3* axis as a potential therapeutic target for improving NPC prognosis.

Oncogene (2026) 45:2225–2236; https://doi.org/10.1038/s41388-026-03792-y

INTRODUCTION

Nasopharyngeal carcinoma (NPC) is a malignant epithelial tumor originating from the inner layer of the nasopharyngeal mucosa, characterized by high invasiveness and metastatic tendency [1]. Despite significant advances in radiotherapy and chemotherapy techniques in recent years, leading to improved local control rates, patients with advanced NPC still face clinical challenges of treatment resistance and distant metastasis [2]. Recent studies have found that this treatment resistance may be closely associated with adaptive survival mechanisms activated by tumor cells under stress conditions [3]. During tumorigenesis and progression, a more hostile microenvironment is created due to "uncontrolled proliferation" and "detachment from the basement membrane for metastasis," manifesting as high metabolic demand, oxidative stress, hypoxia, and nutrient deprivation, among others [4]. Notably, compared to normal cells, highly malignant tumor cells exhibit more efficient response strategies, effectively counteracting and rapidly adapting to various stressors to evade cell death [5]. This suggests that tumor cells may possess unique regulatory systems that reshape the intracellular environment to cope with stress. Therefore, elucidating the mechanisms by which NPC cells survive under stress conditions is of great significance for reversing tumor cell fate and enhancing treatment sensitivity.

When cells are under stress conditions, such as hypoxia, oxidative stress, radiation, chemotherapy, or nutrient deprivation, they can assemble a membrane-less organelle through liquid-liquid phase separation (LLPS), known as stress granules (SGs) [6, 7]. Ras GTPase-activating protein-binding protein 1 (G3BP1) is a core component of the SG [8]. As a central regulatory hub in the SG network, G3BP1 acts as a molecular switch that senses dynamic changes in the concentration of free intracellular RNA, thereby triggering LLPS and SG assembly [9]. Furthermore, SG is closely associated with cellular biological processes and participates in the onset and progression of various human diseases, such as neurodegenerative diseases and malignant tumors [10–12]. It is noteworthy that the mRNAs sequestered in SGs may play a significant role in tumor pathogenesis. It has been reported that SG can capture pre-existing or translationally stalled mRNA [13, 14] and maintain cellular homeostasis by stabilizing mRNA and regulating the expression of pro-survival genes through the redistribution of intracellular resources under stress conditions [15, 16]. Additionally, in tumor cells, the formation of SG is thought to contribute to cellular stress resistance, which can promote tumor cell survival and drive malignant progression [17, 18]. However, the specific functions of these mRNAs in regulating cell fate decisions remain unclear.

To date, significant progress has been made in identifying multiple important types of RNA modifications, such as N6-methyladenosine (m6A), pseudouridine (Ψ), 5-methylcytidine (m5C), and N4-acetylcytidine (ac4C) [19]. These modifications play

[1]Department of Ear, Nose, and Throat, The First Affiliated Hospital of Soochow University, Suzhou, China. [2]Department of Otorhinolaryngology Head and Neck Surgery, Affiliated Hospital of Nantong University, Nantong, China. [3]Institute of Otolaryngology Head and Neck Surgery, Affiliated Hospital of Nantong University, Nantong, China. [4]The Fourth Affiliated Hospital of Soochow University, Suzhou, China. [5]These authors contributed equally: Tian Yue, Haimeng Yin, Ling Yuan. ✉email: zkw1227@163.com; sdfyyljs@sina.com

Received: 16 October 2025 Revised: 19 March 2026 Accepted: 9 April 2026
Published online: 24 April 2026

key roles in regulating mRNA stability, transcription processes, and translation efficiency, thereby influencing various cellular and biological processes [20]. As the sole acetylation event in mRNA modifications, ac4C abundance is comparable to m7G yet remains understudied [21]. N-acetyltransferase 10 (NAT10), which contains both an acetyltransferase domain and an RNA-binding domain, is currently the only identified enzyme known to catalyze ac4C modification [22]. Notably, it was found that high levels of ac4C modification promote mRNA accumulation in the SGs [23]. Additionally, ac4C modulates mRNA stability and translation efficiency to enhance the hypoxic tolerance of gastric cancer cells [24]. These findings provide new insights into the function and consequences of mRNA acetylation, as well as the mechanisms underlying RNA localization in SGs.

This study reveals the core mechanism by which SG promotes NPC progression: under varying survival stress conditions, SG dynamically assembles to specifically enrich ac4C-modified mRNA, implementing precise "sequestration-release" regulation. This mechanism plays a pivotal role in sustaining tumor cell survival.

MATERIALS AND METHODS

Cell culture

Human NPC cell lines (C666-1, TW03(+), CNE2) were cultured at the Institute of Otolaryngology-Head and Neck Surgery, Nantong University Affiliated Hospital (Jiangsu Province, China). All cell lines were confirmed mycoplasma-free and validated through short tandem repeat analysis. Human NPC cell lines were cultured in RPMI 1640 medium (#01-100-ACS; Biological Industries Israel Beit-Haemek, Kibbutz Beit-Haemek, Israel) supplemented with 10% fetal bovine serum (FBS) (#04–001-1ACS; Biological Industries Israel Beit-Haemek) and 1% penicillin-streptomycin Eagle's medium (Biological Industries Israel Beit-Haemek). Cells were grown at 37 °C in 5% CO_2. The cisplatin-resistant CNE-2/DDP cell line was established by chronically exposing the parental CNE-2 cells to gradually increasing concentrations of cisplatin, up to 1.0 μg/mL, over a period of 7 months.

Transfection of lentiviral vectors

Perform transfection according to the previously established protocol [25]. In short, lentiviral vectors and their respective negative controls were generated using the GeneChem software (Shanghai, China). The full-length coding sequence (CDS) of the human G3BP1 gene (NCBI: NM_005754.4) was cloned into the multiple cloning site of the lentiviral overexpression vector pGLV-cmv-mcs-ef1-puro to generate the recombinant plasmid pGLV-cmv-G3BP1-ef1-puro. Gene editing was performed using the CRISPR-Cas9 system with the Lenti-Cas9-puro vector, which carries a puromycin resistance gene and a GFP marker for tracking transfection efficiency. Following transduction, stable cell pools were selected using puromycin. The minimum lethal concentration of puromycin was determined by treating cells with a concentration gradient (e.g., 1, 2.5, 5, and 10 μg/mL) for 48 h. Subsequently, stable monoclonal cell lines were established via 96-well plate limited dilution, and the majority of the selected clones exhibited uniform expression upon validation. The target sequences are provided in Supplementary Table 3.

Western blot

Western blotting was performed using whole-cell lysates. The protein concentration was quantified using a BCA assay kit (cat: 23327, Thermo Fisher Scientific, USA). Protein samples were separated by polyacrylamide gel electrophoresis, transferred to nitrocellulose membranes (cat: ISEQ00010, Millipore, USA), and blocked with blocking buffer. The membranes were then incubated with primary antibodies overnight. The primary antibodies used were as follows: anti-G3BP1 (cat: 13057-2-AP, Proteintech, China), anti-NAT10 (cat: ab194297, Abcam, UK), anti-ATF3 (cat: A13469, ABclonal, China), anti-PARP16 (cat: ab154510, Abcam, UK), anti-PARP10 (cat: 26072-1-AP, Proteintech, China), anti-Cleaved Caspase 3 (cat:25128-1-AP, Proteintech, China), anti-Cleaved PARP (cat: 9541, Cell Signaling Technology, USA), anti-Caspase 3 (cat: ab32351, Abcam, UK), anti-LIG1 (cat: A1858, ABclonal, China), anti-RNF168 (cat: 21393-1-AP, Proteintech, China), and anti-β-actin (cat: ab8226, Abcam, UK). After washing, the membranes were incubated with HRP-conjugated secondary antibodies. Protein bands were visualized using an ECL chemiluminescent substrate (cat: P0018S, Beyotime, China) and analyzed using ImageJ software.

Immunofluorescence assay

Seed cells at a density of 5×10^4 cells per well in 15 mm glass-bottom cell culture dishes (cat: 354469, Corning, USA). After 24 h, wash the cells three times with phosphate-buffered saline (PBS; cat: 10010023, Gibco, USA). Then, fix the cells with 4% paraformaldehyde (cat: BL539A, Biosharp, China) for 20 min at room temperature. Deparaffinize 6-μm paraffin-embedded tissue sections and perform antigen retrieval by heating the slides in Tris-EDTA buffer (pH 9) for 20 min using a Lab Vision PT Module (Thermo Fisher Scientific). After fixation, wash the cells three times with PBS. Permeabilize the cells by incubating them with 0.2% Triton X-100 (cat: ST795, Beyotime, China) for 10 min at room temperature. After permeabilization, wash the cells three times with PBS. Incubate the cells with primary antibodies overnight at 4 °C. Use the following primary antibodies: anti-G3BP1 (cat: ab56574, Abcam, UK), anti-TIA-1 (cat: K109466P, Solarbio, China), anti-MARylation (cat: MABE1076, Millipore, USA), and anti-ac4C (cat: ab252215, Abcam, UK). The next day, wash the cells three times with PBS and then incubate them with appropriate fluorescently labeled secondary antibodies (e.g., cat: A-11008 and A-11001, Thermo Fisher, USA) for 1 h at room temperature in the dark. Finally, mount the samples using an anti-fade mounting medium containing Hoechst dye (cat: 62249, Thermo Fisher Scientific, USA) and image them using fluorescence microscopy.

Cell counting Kit-8

Cell proliferation assays were performed using the CCK-8 assay kit (cat: C0037, Beyotime, China). The procedure was as follows: cell suspensions were seeded into 96-well culture plates (cat: 4515, Corning, USA) and incubated in a 37 °C, 5% CO_2 incubator. After the cells adhered, 10 μL of CCK-8 solution was added to each well, and the plates were incubated for 1–4 h. The optical density (OD) at 450 nm was then measured using a microplate reader at time points of 0, 12, 24, 36, and 48 h. Wells containing only culture medium and CCK-8 solution without cells were used as the blank control. All experiments were performed in triplicate to ensure data reliability.

Real-time tracking of SG dynamics in live cells and in vivo using the small-molecule probe TASG

Cells were seeded in glass-bottomed 96-well plates and cultured overnight. They were first stained for 3 h with a medium containing 2.0 μM TASG probe (cat: P001, Shenzhen Shenlan Technology, China) before being subjected to different stress conditions. Wash away excess probes and drugs with culture medium. Finally, the sample was imaged using a laser scanning confocal microscope/fluorescence microscope. Under excitation at 561 nm, the TASG probe exhibits fluorescence emission in the range of 600–650 nm, allowing for the observation of SGs.

Transmission electron microscope

After centrifugation, the supernatant was discarded, and the cell pellet was collected. The pellet was resuspended and fixed in 2.5% glutaraldehyde at 4 °C for 3 h, followed by low-temperature storage for transport. A 2% low-melting-point agarose solution was prepared and, after cooling to an appropriate temperature, thoroughly mixed with the fixed cell pellet. The mixture was transferred to an embedding mold, cured overnight at 37 °C, and then polymerized at 60 °C for 48 h. Ultrathin sections (60–80 nm) were cut from the fixed specimens using an ultramicrotome and lifted onto 150-mesh copper grids. Finally, the sections were double-stained with uranyl acetate and lead citrate and observed under a transmission electron microscope for image data collection.

Cell proliferation assay

Cells in the logarithmic growth phase were seeded at a density of 5×10^3 cells per well in a 96-well plate. After cell adhesion, the EdU assay was performed following the manufacturer's instructions for the Cell-Light EdU Apollo 567 In Vitro Kit (cat: C10310-1, RiboBio, China). Briefly, cells were incubated with EdU-containing medium for 2 h, fixed, and then subjected to fluorescent staining. EdU-positive cells were observed and counted under a fluorescence microscope, and the cell proliferation rate was calculated. Each experimental group was set up in triplicate, and the entire experiment was repeated three times independently to ensure data reliability.

Tissue microarray samples

NPC tissue microarrays were used by Shanghai Tufei Biotechnology to examine G3BP1, NAT10, and ATF3 expression. All tissue microarray samples used in this study were provided by our collaborating institutions: the Affiliated Hospital of Nantong University and Shanghai Tufei Biotechnology Co., Ltd. The study protocol was approved by the committees for ethical review of research at the Affiliated Hospital of Nantong University. The clinical features of NPC patients are shown in Supplementary Table 1. The prognostic significance of G3BP1, NAT10, and ATF3 was assessed using Kaplan–Meier analysis. Before survival analysis, X-tile software (V.3.6.1, Rimm Lab, Yale School of Medicine) was used to define low and high expression levels of G3BP1, NAT10, and ATF3.

Immunohistochemistry

Formaldehyde-fixed paraffin-embedded (FFPE) sections were initially dried at 60 °C for 1.5–2 h, followed by dewaxing in xylene twice for 15 min each. Sections were then rehydrated by sequential immersion in graded ethanol solutions (100%, 95%, 80%, 70%) and finally in distilled water. Subsequently, antigen retrieval was performed by boiling the sections on slides in sodium citrate buffer. To block endogenous peroxidase activity, sections were treated with 3% hydrogen peroxide, followed by overnight incubation with the primary antibody at 4 °C. The secondary antibody was then applied at room temperature for 1 h, followed by DAB color development and counterstaining with hematoxylin. Two pathologists independently scored protein expression in a blinded fashion. In short, the percentage of tumor cells exhibiting positive staining was designated as follows: 1 (positivity < 10%), 2 (10% < positivity ≤ 30%), 3 (30% < positivity ≤ 70%), and 4 (positivity > 70%). Staining intensity was graded as follows: 1 (no staining), 2 (pale yellow), 3 (brown), and 4 (brown-red). The staining index was calculated by multiplying the proportion of positive tumor cells by the staining intensity. The following primary antibodies were used: G3BP1 (cat:66486-1-Ig, Proteintech, China), Ki67 (cat: 28074-1-AP, Proteintech, China), NAT10 (cat: 13365-1-AP, Proteintech, China), ATF3 (cat: A13469, ABclonal, China).

Mouse

Four- to six-week-old male athymic nude mice were purchased from the Laboratory Animal Center of Nantong University (Jiangsu, China). All animal experiments were conducted in accordance with the guidelines of the Nantong University Laboratory Animal Center and were approved by the Jiangsu Provincial Laboratory Animal Management Committee (Approval No: SYXK(SU)2007-0021).

Nude mouse in vivo model

Mice were randomly assigned to each experimental group, with five mice per group. Each mouse received a subcutaneous injection of 1×10^6 NPC cells from different treatment groups. Animals were monitored every 3 days for survival and tumor formation. Four weeks after injection, mice were euthanized, tumors were excised, and tumor volumes were measured. To investigate the role of differently treated NPC cells in lung metastasis, we established a mouse tumor metastasis model by injecting 2×10^6 luciferase-labeled CNE2 cells, treated under different conditions, into the tail veins of 8-week-old nude mice, with five mice per group. Over a 5-week period, lung metastases were monitored by BLI using the IVIS Lumina Series III (Caliper Life Sciences, Mountain View, CA, USA).

Spot imprinting experiment

First, take 5–10 μg of the RNA sample, denature it at 75 °C for 5 min, and then immediately place it in an ice bath for 1 min. Spot the denatured RNA sample onto a 0.45 μm pore size nylon membrane (Biodyne PALL). Subsequently, two crosslinking treatments were performed using the Stratalinker 2400 UV crosslinker (parameter settings: self-crosslinking mode, 120,000 μJ, 25–50 s). Membrane blocking was performed using a 0.1% PBST solution containing 5% skim milk powder at room temperature for 1 h. The incubation condition for the ac4C antibody was overnight at 4 °C (cat: ab252215, Abcam diluted 1:1000). After three 5-min washes with PBST, the membrane was incubated with HRP-labeled rabbit secondary antibody (1:10,000) at room temperature for 1 h. After washing, perform exposure detection using the Hyperfilm ECL development system for the appropriate duration. Finally, stain the membrane with 0.01% methylene blue for 1 h, then wash with RNase-free water for 1 h.

Acetylated RNA immunoprecipitation sequencing

Acetylated RNA immunoprecipitation sequencing (acRIP-seq) and downstream data analysis were performed by Guangzhou Epigenomics Technology Co., Ltd. acRIP-seq was carried out on control and 36-h starvation C666-1 cells, with three independent biological replicates per group. Briefly, total RNA was extracted using TRIzol reagent (cat: 15596018CN, Thermo Fisher Scientific, USA). 100 μg of RNA was fragmented to 100–200 nt by incubation with 10× RNA Fragmentation Buffer (100 mM Tris-HCl, 100 mM $ZnCl_2$, nuclease-free H_2O) at 70 °C for 5 min. The reaction was stopped by adding 0.5 M EDTA to a final concentration of 50 mM. Fragmented RNA was immunoprecipitated with anti-ac4C monoclonal antibody at 4 °C for 2 h following the manufacturer's instructions of the EpiTM ac4C Immunoprecipitation Kit (cat: R1815, Epibiotek, China). Input (non-IP) and ac4C-IP samples were used to construct libraries using an automated workflow and subjected to 150-bp paired-end sequencing on an Illumina NovaSeq 6000.

RNA sequencing

RNA sequencing (RNA-seq) and data analysis were performed by Guangzhou Epigenomics Technology Co., Ltd. RNA-seq was performed on cells from the control group and the 36-h starvation group of C666-1, with three independent biological replicates per group. Following the instructions, library preparation was performed using the VAHTS Stranded mRNA-seq Library Preparation Kit (cat: NR612-02, Vazyme Biotech, China) with Illumina NovaSeq 6000 V2, followed by computational analysis.

Extraction of SG RNA and ac4C RIP-seq

The extraction of the SG core refers to these two papers [26, 27]. In brief, C666-1 cells stably expressing G3BP1-GFP were cultured to ~80% confluence and then subjected to either 36 h of starvation or 1 h of $NaAsO_2$ treatment to induce stress granule formation. Cells were subsequently harvested by centrifugation, rapidly frozen in liquid nitrogen, and stored at −80 °C. Cell pellets were resuspended in SG lysis buffer containing protease/nuclease inhibitors. After repeated pipetting to lyse cells, SG core pellets were enriched by centrifugation at $18{,}000 \times g$ for 20 min at 4 °C. Following washing, pellets were resuspended in 300 μL lysis buffer. The lysate was pretreated twice with dynabeads, magnetic beads, to remove nonspecific binders. Subsequently, anti-N4-acetylcytidine (ac4C) antibody (cat: ab252215, abcam,UK) was added and incubated at 4 °C for 1 h or overnight. After centrifugation to remove excess antibody, 60 μL of magnetic beads were added and incubated at 4 °C for 3 h. The magnetic bead complexes were sequentially washed with three detergent buffers (containing NaCl, urea, etc.). Finally, RNA was released by proteinase K digestion (37 °C for 15 min) and extracted using the Trizol method for subsequent analysis. Extraction of SG RNA and ac4C RIP-seq analysis were performed by Guangzhou Epigenomics Technology Co., Ltd.

Real-time quantitative PCR analysis

First, extract total RNA from NPC cells using the TRIzol reagent (cat:15596018, Thermo Fisher Scientific, USA) according to the manufacturer's instructions. Subsequently, RNA was reverse transcribed into cDNA using a reverse transcription kit (cat: K1622, Thermo Fisher Scientific, USA). qPCR amplification was performed using SYBR Green premix reagent (cat: 04913914001, Roche, CH). Primer sequences are listed in Supplementary Table 4.

RNA fluorescence in situ hybridization

The experiment was performed according to the manufacturer's instructions (cat: H0101, GENESEED, China). First, 5×10^4 cells were seeded into a 15 mm glass-bottom dish. After cell adhesion, cells were fixed with 4% paraformaldehyde at room temperature for 15 min and rinsed thoroughly with PBS. Membrane permeabilization and blocking were performed sequentially with Solution A (15 min), Solution B (15 min), and Solution C (15 min). After PBS washing, samples were refixed with 4% paraformaldehyde for 10 min and rinsed. Pre-hybridization was performed by incubating the samples in hybridization buffer at 55 °C for 2 h. The RNA FISH probe mix-Cy3 was purchased from Gien Biotechnology Co., Ltd. For probe hybridization, the probe was diluted 1:50–1:200 in hybridization buffer, denatured at 85 °C for 3 min, and immediately transferred to an ice bath. After equilibration at 37 °C, the probe mixture was applied to the samples and hybridized in the dark at 37–42 °C for 18–72 h. After hybridization, samples were washed with 1× Washing Buffer at 42 °C for 2 min, followed by a room-temperature wash for 8 min. For subsequent immunofluorescence staining, samples were incubated sequentially with a primary antibody against G3BP1 (cat: 13057-2-AP, Proteintech, China) and the corresponding secondary antibody. Finally, slides were mounted with a

DAPI-containing anti-fade mounting medium in the dark for 15 min, observed under a fluorescence microscope, and images were captured for analysis.

Comet assay

Single-cell gel electrophoresis was performed using the DNA Damage Comet Assay Kit (cat: KGA1302, KeyGEN, China) according to the manufacturer's instructions. A 1% normal-melting-point agarose base layer (100 μL) was cast first. A second layer consisting of 75 μL 0.7% low-melting-point agarose mixed with ~10^4 cells was added. After solidification, a third layer of 75 μL 0.7% low-melting-point agarose was applied. The slides were immersed in pre-chilled lysis buffer and incubated at 4 °C for 3 h. They were then placed in freshly prepared alkaline electrophoresis buffer for 1 h, followed by electrophoresis at 25 V and 300 mA for 20 min. Slides were neutralized by three 10-min washes in 0.4 M Tris buffer (pH 7.5) at 4 °C. Each gel was stained with 20 μL propidium iodide (PI) solution, covered with a coverslip, and incubated in the dark for 10 min. DNA was visualized as red fluorescence (excitation 515–560 nm) under a fluorescence microscope, enabling clear identification of nuclear and migrated DNA.

CHIP assay

ChIP experiments were performed using a commercial ChIP assay kit (Thermo Fisher Scientific, #27177). The specific procedure is as follows: C666-1 cells in the growth phase were fixed with formaldehyde and subjected to ultrasonication to fragment chromatin. Subsequently, DNA-protein complexes were immunoprecipitated using antibody-conjugated agarose beads. Subsequent steps included crosslink reversal and DNA purification. Finally, 10 μL of the resulting PCR product was analyzed by gel electrophoresis. Primer sequences are listed in Supplementary Table 5.

Multivariate regression analysis

Based on a predefined set of covariates, a full model incorporating all variables was constructed. For survival data, the Cox proportional hazards model was employed, with its proportional hazards assumption validated. Model results were reported as adjusted hazard ratios with 95% confidence intervals. Multivariate regression analysis was used to control for confounding effects, and all statistical analyses were performed using SPSS software.

Data analysis

Statistical analyses were performed using Prism V.6 (Boston, Massachusetts, USA) and SPSS V.19.0 (IBM, USA). Experimental data were derived from at least three independent experiments and are presented as mean ± standard deviation. Spearman's rank correlation coefficient was used for correlation analysis. Statistical significance was determined using two-tailed *t*-tests and one-way analysis of variance (ANOVA), with significance levels denoted as follows: $^{*}p < 0.05$, $^{**}p < 0.01$, $^{***}p < 0.001$, and $^{****}p < 0.0001$.

RESULTS

Protein mono-ADP-ribosylation partially regulates SG formation

To investigate the effects of different stress conditions on SG formation in NPC, we simulated adverse survival conditions in the tumor microenvironment by subjecting cells to nutrient deprivation and hypoxia treatment [4]. The results showed that the expression level of G3BP1, a core regulatory protein of SG, was significantly upregulated under both starvation and hypoxia stress conditions (Fig. 1A, B). Further immunofluorescence (IF) staining analysis revealed that both SGs core proteins, G3BP1 and TIA-1, formed distinct granular aggregates in cells under starvation or hypoxia stress, compared to unstressed controls, indicating widespread SGs formation. (Fig. 1C, D and Supplementary Fig. S1A–F). Transmission electron microscopy (TEM) further revealed that both the diameter and number of SGs were significantly increased in cells subjected to starvation treatment (Fig. 1E, F). Critically, and consistent with our in vitro observations, IF staining of tissue sections from NPC patients confirmed the presence of SGs within the tumor microenvironment (Supplementary Fig. S1G). This finding suggests that adverse environmental stressors within the tumor microenvironment may induce the formation of SGs.

Given that mono-ADP-ribosylation (MARylation) is critical for multiple stress responses [28], we therefore explored its impact on SGs assembly and maintenance. MARylation is a reversible post-translational modification catalyzed by members of the poly ADP-ribose polymerase (PARP) family [29]. This process participates in regulating various physiological and pathological processes, including DNA damage repair and cellular stress responses, by transferring a single ADP-ribose subunit from the donor nicotinamide adenine dinucleotide (NAD+) to the target protein [30–32]. Within the PARP family, most members are monoenzymes primarily responsible for mediating the MARylation of substrates and are mainly localized in the cytoplasm [33]. Moreover, PARP overexpression has been shown to induce SG assembly [34, 35], suggesting that MARylation may play a crucial role in the dynamic regulation of SG.

To investigate the role of MARylation in stress granule assembly, we treated cells with the pan-PARP inhibitor OUL232 [36], which effectively targets multiple PARP family members including PARP10 and PARP16 and concomitantly reduced the stress-enhanced MAR-specific IF signal (Supplementary Fig. S1H–J). IF analysis demonstrated that treatment with either OUL232 or Compound C108, a G3BP2 inhibitor [37], significantly reduced the percentage of cells positive for SG (Fig. 1G, H, Supplementary Figs. S1K, S2A–F). Concordantly, OUL232 blunted the stress-induced rise of the SGs scaffold protein G3BP1 (Supplementary Fig. S1M, N) and reduced SGs fusion events tracked by live-cell fluorescent probes (Fig. 1I). Further validation through knockdown of other individual PARP members revealed that downregulation of both PARP10 and PARP14 similarly suppressed SGs formation in NPC cells (Supplementary Fig. S2G). Collectively, these findings demonstrate the pivotal role of single ADP-ribosylation in regulating SGs formation in NPC cells.

EdU and CCK-8 assays revealed that under stress conditions, NPC cells treated with either Compound C108 or OUL232 exhibited reduced proliferative capacity (Supplementary Fig. S3A–C, F) and showed a marked increase in the expression of apoptosis markers, including Cleaved PARP, Cleaved Caspase-3, and caspase-3 (Supplementary Fig. S3D, E). Furthermore, these treatment groups exhibited a relatively higher DNA tail percentage, indicating that inhibition of stress granule assembly also impairs DNA damage repair (Supplementary Fig. S3G, H). These results indicate that MAR-mediated stress granule formation represents not merely a stress response, but a critical adaptive mechanism that supports the survival of NPC cells under adverse conditions.

The SG core protein G3BP1 promotes NPC progression and predicts poor prognosis

To further investigate the clinical significance of G3BP1, immunohistochemical (IHC) staining and G3BP1 expression analysis were performed on NPC tissue microarrays ($n = 111$). As shown in Fig. 2A–C, upregulation of G3BP1 was positively correlated with distant metastasis (Supplementary Table 1). Analysis based on IHC scores and TNM staging revealed that patients with stage III and IV had significantly higher G3BP1 expression levels than those with stage I (Fig. 2D). Furthermore, patients whose scores ranged from 9 to 16 were classified as having high G3BP1 expression ($n = 61$), whereas those with scores of 1–8 were classified as low expression ($n = 50$). Kaplan–Meier survival analysis indicated that patients with high G3BP1 expression had a significantly shorter overall survival (Fig. 2E). These findings indicate that the SG core protein G3BP1 promotes NPC progression and is associated with poor prognosis.

To further explore whether *G3BP1* promotes NPC progression, a mouse xenograft model was established by implanting control cells, *G3BP1*-overexpressing cells, and Compound C108-treated C666-1 cells. Overexpression was achieved by infection with green fluorescent protein (GFP)-tagged *G3BP1* lentivirus, and

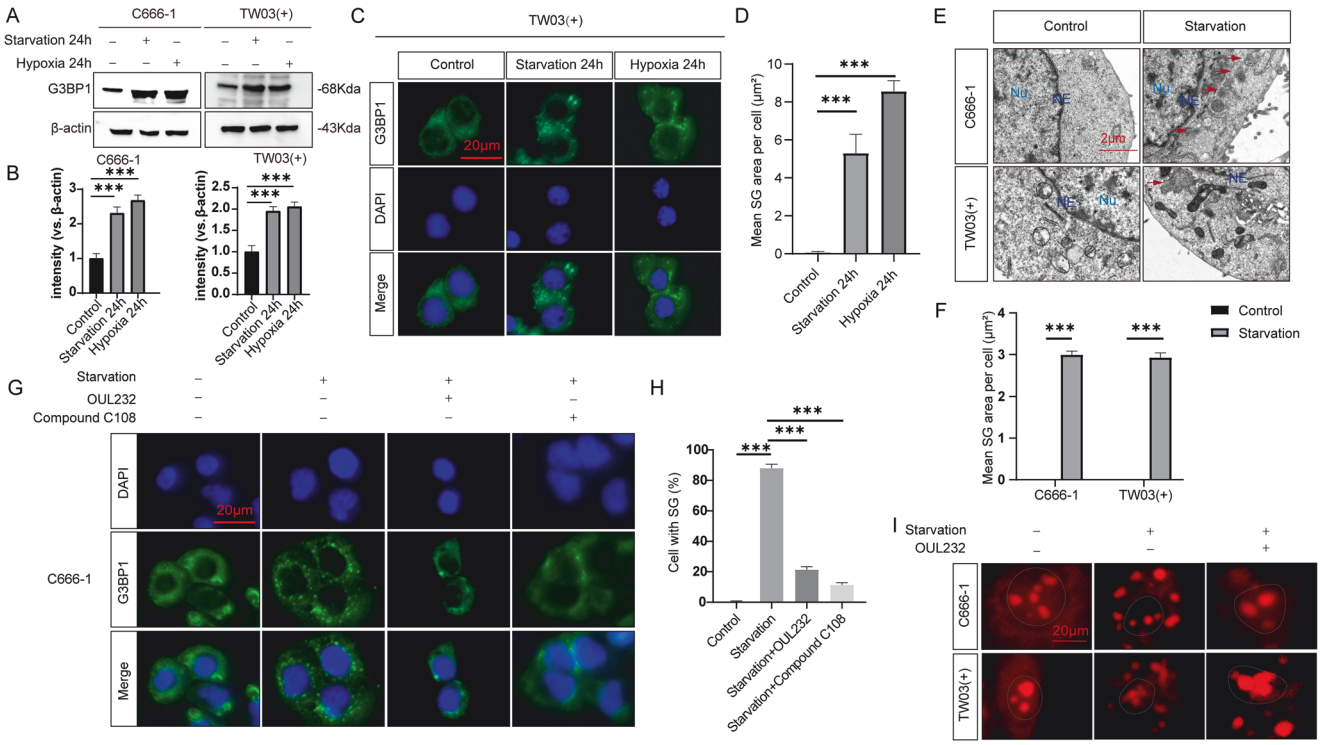

Fig. 1 MARylation is essential for SG assembly. Stress culture conditions: Hypoxia treatment: Cells were placed in sealed culture containers provided by Mitsubishi Corporation and cultured under 1% O_2 conditions for 24 h. Starvation treatment: Cells were cultured for 24 h in amino acid-free 1640 basal medium. **A** Western blot analysis detected the expression of SG core protein G3BP1 in C666- 1 and TW03(+) cells across the control group and various stress groups (starvation 24 h and hypoxia 24 h). **B** Perform quantitative analysis of Western blot results using ImageJ software (one-way ANOVA). **C** TW03(+) cells under control and stress conditions (24 h starvation and 24 h hypoxia), showing representative IF images of G3BP1 (green) and DAPI (blue). Scale bar, 20 μm. **D** Quantify the mean area of SGs in each cell using ImageJ software (one-way ANOVA). **E** Transmission electron microscopy analysis of SGs under control vs. 24 h starvation conditions. Scale bar, 2 μm. **F** Quantify the mean area of SGs in each cell using ImageJ software (one-way ANOVA). **G** Representative IF images of SG formation in cells treated with OUL232 (3.4 μM, 24 h) or compound C108 (4 μM, 48 h) under stress conditions. Scale bar, 20 μm. **H** Quantify the percentage of cell with SG using ImageJ software (one-way ANOVA). **I** TASG monitors the dissipation process of SG. Scale bar, 20 μm. All experiments were repeated three times. Data are expressed as mean ± standard deviation. *$P < 0.05$, **$P < 0.01$, ***$P < 0.001$.

efficiency was validated by western blot analysis (Supplementary Fig. S2H, I). In the xenograft model, mice implanted with Compound C108-treated cells exhibited significantly smaller tumor volume and weight, as well as a reduced proportion of Ki67-positive cells, compared with the control group (Fig. 2F–J). Conversely, *G3BP1*-overexpressing xenografts demonstrated enhanced tumorigenic capacity and a higher Ki67 index (Fig. 2F–J). Furthermore, immunofluorescence analysis of tumor tissue sections from nude mice revealed that the G3BP1-overexpressing group exhibited the highest proportion of cells containing stress granules, whereas the group treated with Compound C108 showed the lowest percentage of SG-positive cells (Fig. 2K, L). Overall, our in vivo data reveal that *G3BP1* is essential for driving NPC proliferation.

Stress-induced ac4C modification mediated by NAT10 promotes mRNA localization to SGs

SGs are enriched with ac4C-modified RNA, and this enrichment increases significantly under oxidative stress [23]. Acetylation of RNA may influence mRNA localization within the SG by regulating the translation release process of mRNA from the ribosome [38]. These findings provide new avenues for research into the biological functions of mRNA acetylation. Consistent with this observation, both NAT10 expression levels and ac4C modification abundance increased under stress conditions of starvation or hypoxia (Fig. 3A–C), exhibiting a sustained upward trend as stress duration prolonged (Fig. 3D–F). Notably, upon removal of the stress conditions, both NAT10 expression and ac4C modification levels gradually returned to baseline states (Fig. 3D–H). To validate the functional reversibility and translation dependency of ac4C-associated SGs, we established a hypoxia-induced model and co-administered the translation inhibitor CHX during stress recovery. Results demonstrated that CHX treatment accelerated the dissolution of SGs during the recovery phase, indicating that their dissolution process depends on active translation (Supplementary Fig. S4A, B). This confirms the reversible nature of ac4C-enriched granules. These results indicate that ac4C acetylation is a dynamic response to cellular stress, being specifically upregulated during stress, which implies a crucial role for this modification in regulating cellular stress responses.

IF showed that under non-stress conditions, ac4C was primarily localized to the nucleolus, consistent with its role in basal RNA metabolism. However, under starvation or hypoxia, ac4C exhibited significant colocalization with G3BP1 (Fig. 3I, J and Supplementary Fig. S4E). This stress-induced relocalization suggests that ac4C-modified RNAs are actively recruited to SGs to meet the cell's demand for RNA protection under adverse conditions. To investigate the effect of *NAT10* on SG composition, we generated a *NAT10* knockout C666-1 cell line using CRISPR-Cas9 technology and validated the knockout efficiency by Western blot (Supplementary Fig. S4C, D). Comparing WT and *NAT10* KO cells revealed that both forms can form SG under stress conditions, but *NAT10* deficiency resulted in significantly reduced levels of ac4C modification within SGs (Fig. 3K, L and Supplementary Fig. S4F, G). These findings indicate that under nutritional deprivation or hypoxic stress conditions, ac4C modification can be recruited specifically to SGs, promoting the targeted transport of acetylated

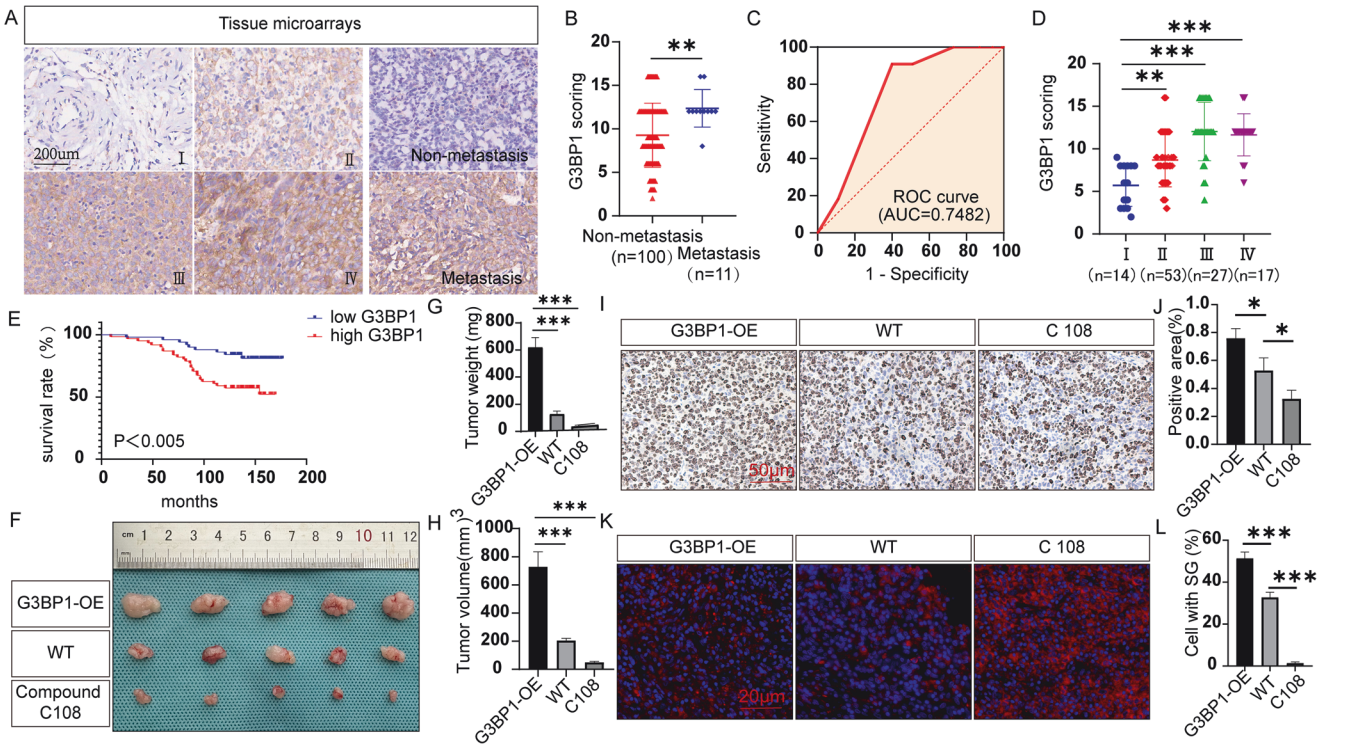

Fig. 2 The SG core protein G3BP1 promotes NPC progression and predicts poor prognosis. A Representative IHC staining of G3BP1 in NPC tissue chips ($n = 111$, scale bar, 200 μm). **B** The statistical comparison of G3BP1 scores between the two groups (Student's *t* test). **C** A receiver operating characteristic (ROC) curve was plotted to validate the predictive accuracy of G3BP1 expression in metastatic nasopharyngeal carcinoma (ROC AUC = 0.7482). **D** Statistical comparisons of G3BP1 expression levels across different clinical stages (one-way ANOVA). **E** Patients were divided into high-expression and low-expression groups based on the median level of G3BP1 expression. Overall survival was compared between the two groups using Kaplan–Meier analysis (log rank test). **F** Macrographic image of an NPC xenograft tumor. **G**, **H** Analysis of weight and volume of xenograft tumors derived from NPC across different experimental groups. **I** IHC detection of Ki67 expression. Scale bar, 50 μm. **J** Quantification of IHC staining for Ki67 expression was conducted using One-way ANOVA. **K** Immunofluorescence staining of G3BP1 in tumor tissue sections from nude mice. **L** Quantify the percentage of cell with SG using ImageJ software (one-way ANOVA). Data are expressed as mean ± standard deviation. $^{*}P < 0.05$, $^{**}P < 0.01$, $^{***}P < 0.001$.

RNA to SGs. Notably, depletion of *NAT10* does not affect SG formation or its morphological characteristics, suggesting that ac4C modification primarily contributes to the precise localization of mRNA within SGs rather than being essential for SG assembly. In summary, NAT10-mediated ac4C modification plays a crucial role in the subcellular localization of mRNA, enabling the selective enrichment of specific mRNAs into SGs under stress conditions.

To investigate the regulatory role of ac4C-modified mRNA mediated by NAT10 in NPC survival, we established a subcutaneous xenograft model in nude mice. WT cells or *NAT10* KO C666-1 cells were subcutaneously implanted into male nude mice. One week post-implantation, one group of C666-1 cell-implanted experimental mice received intraperitoneal injections of the NAT10-specific inhibitor remodelin (20 mg/kg) every other day for 4 weeks [39]. Data indicated that compared with the shNC control group, tumor growth was significantly suppressed in both the *NAT10* knockdown group and the remodelin group. This was demonstrated by a reduction in tumor volume and weight (Fig. 3M, N) and confirmed by decreased Ki-67 staining, indicating a low cell proliferation rate (Supplementary Fig. S4H). These results demonstrate the pivotal role of the NAT10-ac4C axis in the NPC stress response, highlighting its potential as a target for novel RNA-modification-based antitumor therapies.

Under stress conditions, ATF3, RNF168, and LIG1, which are involved in DNA damage repair, preferentially respond to ac4C acetylation modification

To further investigate the biological function of mRNA acetylation modifications in SGs, we performed a combined analysis of acetylated RNA immunoprecipitation sequencing (acRIP-seq) and mRNA sequencing (mRNA-seq) using control and 36-hour starved C666-1 cells to identify potential ac4C-modified mRNA targets recruited during stress in NPC (Fig. 4A). Evaluation of ac4C modifications revealed a substantial increase in the enrichment of ac4C motifs under stress conditions, particularly the "CXXCXXCXX" motif (Fig. 4B). We observed the accumulation of ac4C sites near translation initiation sites under stress, with most sites located within coding sequences (Fig. 4C). The wild-type (WT) group exhibited 4902 unique ac4C modification peaks and 3,555 unique ac4C genes, while the starvation group showed 29,296 unique ac4C modification peaks and 10,458 unique ac4C genes (Fig. 4D, E). Gene ontology analysis revealed that differentially expressed genes in the starvation-treated group were significantly enriched in multiple biological processes, including DNA damage repair pathways such as mismatch repair (Supplementary Fig. S5A). Furthermore, correlation analysis of gene expression profiles revealed significant upregulation of DNA damage response (DDR) mRNAs, including Activating Transcription Factor 3 (ATF3), Ring Finger Protein 168 (RNF168), and DNA Ligase 1 (LIG1), with ATF3 showing the most pronounced difference (Fig. 4F). This finding was further supported by Integrated Genomics Viewer (IGV) profiles, which showed a marked increase in ac4C modification peaks on the *LIG1*, *RNF168*, and *ATF3* genes (Fig. 4G and Supplementary Fig. S5B).

Notably, through integrated analysis of acRIP-seq and mRNA-seq data, we identified a total of 42 differentially expressed genes ($|\log2FC| > 1$, FDR < 0.05), including 23 hyperacetylated up-

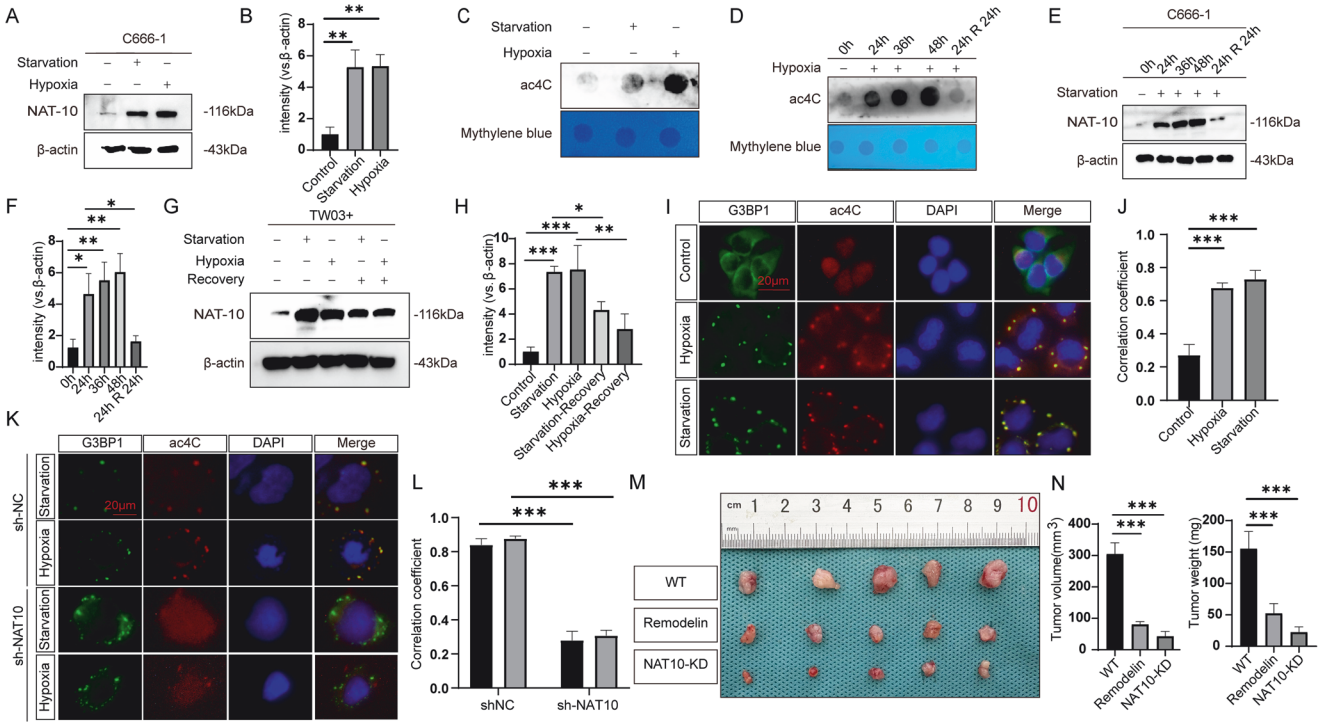

Fig. 3 Stress-induced ac4C modification mediated by NAT10 promotes mRNA localization to SGs. A Western blot detection of NAT10 expression levels under stress conditions. **B** Quantification of western blot results using ImageJ software (one-way ANOVA). **C** Dot blot analysis of mRNA ac4C modification abundance in C666-1 cells under stress conditions (starvation and hypoxia). **D** Dot blot analysis of mRNA ac4C modification abundance in TW03(+) cells at different hypoxia durations. **E** Western blot detection of NAT10 expression levels in C666-1 cells at different starvation time points. **F** Quantification of western blot results using ImageJ software (one-way ANOVA). **G** Western blot detection of NAT10 expression levels during stress and after stress relief. **H** Quantification of western blot results using ImageJ software (one-way ANOVA). **I** IF analysis of the colocalization between ac4C and the SG core protein G3BP1 under different stress conditions (starvation 24 h and hypoxia 24 h) Scale bar, 20 μm. **J** Pearson correlation analysis revealed the co-localization of SG (G3BP1) with ac4C under different stress conditions (starvation and hypoxia). **K** Knockout of NAT10 in C666-1 cells, followed by IF detection of the co-localization between ac4C and SGs under stress conditions. **L** Pearson correlation analysis revealed the co-localization of SG (G3BP1) with ac4C under stress conditions in NAT10-knockout C666-1 cells. **M** Macroscopic images of NPC xenograft tumors. **N** Analysis of the weight and volume of NPC-derived xenograft tumors across different experimental groups (one-way ANOVA). All experiments were repeated three times. Data are expressed as mean ± standard deviation. $^{*}P < 0.05$, $^{**}P < 0.01$, $^{***}P < 0.001$.

regulated genes (Fig. 4H). More importantly, we extracted RNA from SGs for ac4C RIP-seq analysis and integrated the results with the aforementioned acRIP-seq and RNA-seq data. This revealed that ATF3, which is highly modified by ac4C, not only showed significant upregulation under stress conditions but was also enriched in SGs (Fig. 4H and Supplementary Fig. S5C). Further validation via SG ac4C RIP-qPCR verified the stress-dependent association of ATF3, LIG1, and RNF168 mRNAs with SGs (Fig. 4I and Supplementary Fig. S5D, E). These findings suggest that under stress conditions, ATF3 may be recruited to SGs through NAT10-mediated ac4C acetylation, thereby facilitating a rapid and robust cellular stress response.

Remobilization of SG-stored mRNAs for DNA repair after stress resolution

Given that SGs selectively enrich and protect untranslated mRNAs and regulatory proteins under stress, releasing these mRNAs to resume translation upon stress resolution [40], we observed through RNA immunofluorescence experiments that ATF3, RNF168, and LIG1 colocalized with SGs under starvation conditions. This colocalization was lost upon stress resolution (Fig. 5A, B and Supplementary Fig. S6A). Notably, the expression levels of key repair factors ATF3, LIG1, and RNF168 were significantly upregulated following stress resolution (Fig. 5C, D and Supplementary Fig. S6B, C). Concurrently, comet assay results demonstrated that the percentage of DNA tails decreased significantly after stress resolution compared to during stress, indicating reduced DNA damage (Fig. 5G, H). These findings suggest that, following stress resolution, mRNAs stored within SGs are released and translated. These DDR-related mRNAs may promote NPC cell survival by participating in DNA damage repair processes. Further studies revealed that both *NAT10* gene knockout and treatment with OUL232 or Compound C108 resulted in significantly reduced expression of ATF3, LIG1, and RNF168 during the stress recovery phase (Fig. 5E, F and Supplementary Fig. S6D–F). Additionally, these treatment groups exhibited a relatively high percentage of DNA tails (Fig. 5G, H). These findings suggest that NAT10-dependent ac4C modification may promote the targeting of DNA damage repair-related mRNAs to the SGs, ensuring their stable storage under stress. Moreover, MARylation may influence mRNA protection efficiency by regulating SG assembly. When these mechanisms are disrupted, the mRNAs encoding key repair factors cannot be effectively sheltered during stress, leading to impaired translation restart after stress resolution and consequently compromising DNA damage repair capacity.

The *G3BP1/NAT10/ATF3* axis is highly expressed in NPC tissues and positively correlates with disease progression

Given that ATF3 is a transcription factor, we first used the JASPAR database to predict its potential binding sites in the promoters of *LIG1* and *RNF168* (Supplementary Fig. S7A). To confirm this bioinformatic prediction, we performed chromatin immunoprecipitation followed by qPCR (ChIP-qPCR). The results demonstrated significant enrichment of ATF3 at these predicted promoter

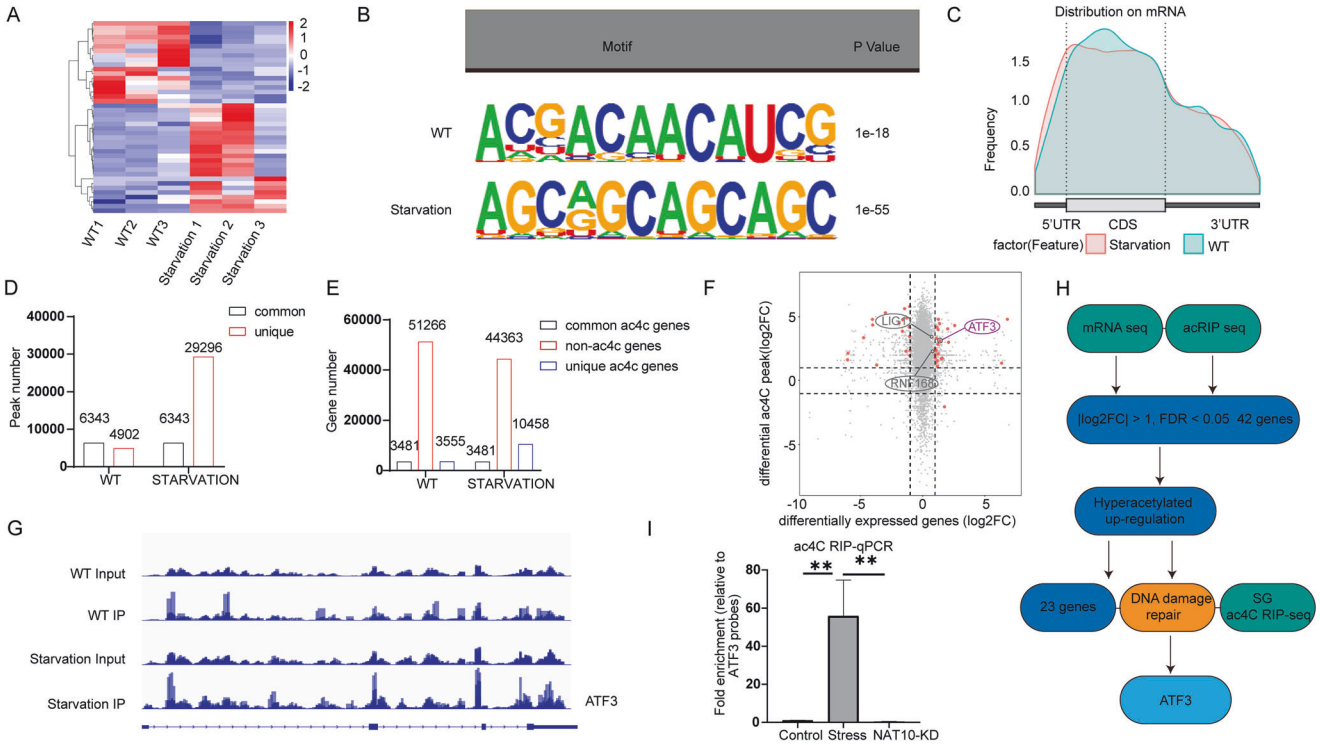

Fig. 4 ATF3 preferentially responds to ac4C acetylation modification in DNA damage repair under stress conditions. A Heatmap combining acRIP-seq and RNA-seq data illustrates the differential expression of ac4C-associated RNAs in C666-1 cells between the control and starvation groups. **B** Sequence analysis of motifs highly enriched within ac4C peaks in acRIP-seq. **C** The predominant distribution of ac4C peaks is observed in the coding sequence (CDS) region. **D** Quantify the number of ac4C peaks present in wild-type (WT) and starved C666-1 cells using ac4C-seq. **E** Quantification of ac4C-modified transcripts in C666-1 cells using the ac4C-seq method in the wild-type (WT) and starvation groups. **F** Ac4C quadrant distribution diagram, emphasizing hyperacetylation of upregulated genes. **G** The Integrative Genomics Viewer displays the distribution of ac4C peaks from acRIP. **H** Bioinformatics analysis workflow for stress downstream targets. **I** SG ac4C RIP-qPCR analysis confirmed that stress conditions elevated the ac4C modification level of ATF3 mRNA, and this induction was abolished by NAT10 knockout. Data are expressed as mean ± standard deviation. $^{*}P < 0.05$, $^{**}P < 0.01$, $^{***}P < 0.001$.

regions (Supplementary Fig. S7B), providing direct evidence for its physical association with these target genes. To further investigate the clinical significance of the G3BP1/NAT10/ATF3 axis, we performed immunohistochemical analysis on tissue microarrays comprising 111 samples of NPC. Based on staining scores and TNM staging, the results demonstrated significantly higher expression levels of NAT10 and ATF3 in stage III and IV patients compared to those in stage I (Fig. 6A–C). Furthermore, the upregulation of NAT10 and ATF3 expression was positively correlated with distant metastasis and tumor recurrence (Fig. 6D, E and Supplementary Fig. S7C–F). Kaplan–Meier survival analysis revealed that high expression of NAT10 and ATF3 was significantly associated with poorer overall survival in NPC patients (Fig. 6F, G). Using immunohistochemical scoring, we confirmed that ATF3 positively correlates with NAT10 and G3BP1, while NAT10 positively correlates with G3BP1 (Fig. 6H, I and Supplementary Fig. S7G). Multivariable Cox regression analysis identified the G3BP1/NAT10/ATF3 axis as an independent prognostic factor, with the composite Gene Score (sum of G3BP1, NAT10, and ATF3 scores) showing a significant association with overall survival (HR = 1.044, 95% CI 1.001–1.090, $p = 0.043$). This result indicates that each unit increase in the Gene Score corresponds to an approximate 4.4% increase in mortality risk (Supplementary Table 2). In the metastasis model, G3BP1 overexpression significantly promoted lung metastasis, as indicated by enhanced bioluminescence signals. In contrast, the metastatic burden was markedly suppressed by G3BP1 overexpression in combination with ATF3 knockout, NAT10 knockout, or treatment with compound C108 (Fig. 6J, K). Furthermore, to investigate the role of this axis in therapeutic resistance, we established a cisplatin-resistant NPC cell line (CNE-2/DDP) through chronic, stepwise exposure of parental CNE-2 cells to cisplatin. In subcutaneous xenograft models, treatment with C108 effectively resensitized CNE-2/DDP tumors to cisplatin (Fig. 6L–N). Collectively, these data demonstrate that stress granule-mediated activation of the G3BP1/NAT10/ATF3 axis plays a pivotal role in DNA damage repair. This axis not only drives tumor progression and metastasis but also contributes to cisplatin resistance in NPC—thus representing a potentially valuable prognostic biomarker for NPC.

DISCUSSION

SG assembly is a dynamically regulated process influenced by multiple factors, including external stress stimuli, post-translational protein modifications, RNA modifications, and intermolecular interactions [23, 41–44]. Increasing evidence indicates that aberrant regulation of SGs is closely associated with the onset and progression of various human diseases, including NPC [45]. The formation of SGs can help cancer cells adapt to stressful conditions such as chemotherapy, hypoxia, and nutrient deprivation, enhancing their survival capacity by inhibiting apoptosis and promoting metabolic reprogramming [46]. However, little is known about the impact of SG components on NPC progression. Our study shows that G3BP1, as a key assembly factor of SGs, plays an important pro-cancer role in NPC. Further research reveals that ac4C-modified mRNAs of ATF3, RNF168, LIG1, and others preferentially localize to SGs under stress conditions. Following tumor neovascularization and the concomitant alleviation of cellular stress, a subset of the sequestered mRNAs within SGs is released. The subsequent translation of these mRNAs contributes

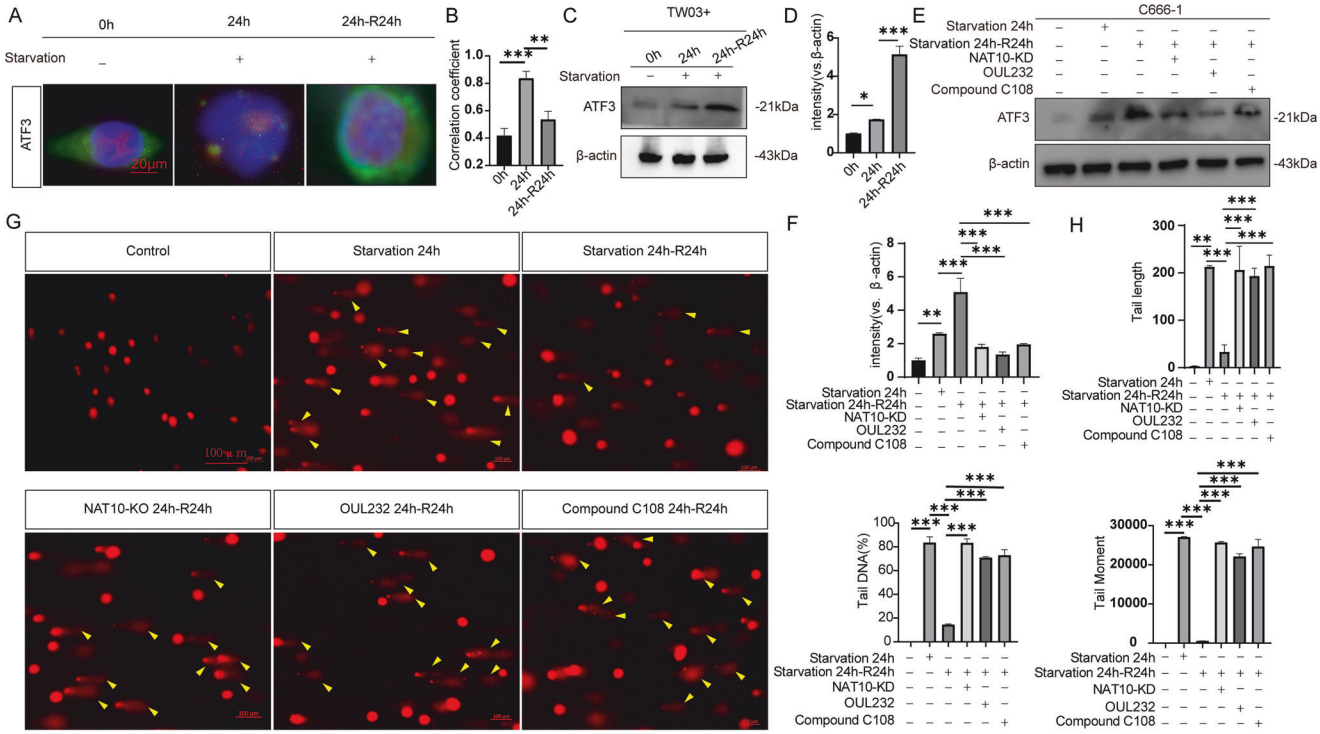

Fig. 5 Following stress resolution, mRNA stored in SGs resumes translation, actively participates in DNA damage repair, and promotes the survival of NPC cells. A Colocalization of ATF3 and SGs during RNA fluorescence in situ hybridization under stress conditions and after stress resolution. **B** Pearson correlation analysis revealed the colocalization of ATF3 and SGs during RNA fluorescence in situ hybridization under stress conditions and after stress resolution. **C** Western blot detection of ATF3 protein expression in TW03(+) cells under stress conditions and after stress resolution. **D** Quantification of western blot results using ImageJ software (one-way ANOVA). **E** Western blot detection of ATF3 protein expression in C666-1 cells under stress conditions, post-stress recovery, and in post-stress recovery groups treated with NAT10 knockout, OUL232, or Compound C108. **F** Quantification of western blot results using ImageJ software (one-way ANOVA). **G** Representative comet assay images showing DNA damage in each experimental group. **H** Analysis of DNA damage assessed by the comet assay. All experiments were repeated three times. All data are expressed as mean ± standard deviation. $^{*}P < 0.05$, $^{**}P < 0.01$, $^{***}P < 0.001$.

to DNA damage repair, thereby ultimately promoting NPC survival and malignant progression (Fig. 7).

Previous studies have established that MARylation of ribosomal proteins suppresses translation initiation by stabilizing eIF6-ribosome interactions [47]. Given that SGs are membrane-less organelles specifically formed by LLPS of mRNA-protein complexes following translational stalling [47], we initially hypothesized that MARylation provides the essential biochemical trigger for SG nucleation by rapidly modifying components of the translation machinery during early cellular stress. Interestingly, consistent with previous findings [35, 48], our data demonstrate that genetic ablation of mono-ADP-ribosyltransferases (mono-ARTs) PARP10 and PARP14, or pharmacological inhibition of their catalytic activity, significantly attenuates SG assembly in NPC cells, establishing MARylation as a critical "molecular switch" governing SG biogenesis. Consequently, inhibition of MARylation likely compromises stress adaptation, thereby enhancing chemosensitivity. Future proteomic interrogation of SG-associated MARylated substrates and functional characterization of PARP10/14-specific signaling networks will be instrumental in delineating the full regulatory scope of this axis and may reveal novel therapeutic targets for circumventing SG-mediated drug resistance.

Current research on stress-induced SGs primarily focuses on their assembly-disassembly kinetics, while studies on SG components remain limited. As RNA biology advances, researchers have discovered that mRNA—characterized by rapid metabolism and a short half-life—serves not only as a "messenger" but also carries multiple post-transcriptional modifications [19]. Notably, under oxidative stress, ac4C-modified RNA shows significant enrichment within SGs (~4.2-fold), whereas other common mRNA modifications, such as m6A and m7G, do not exhibit comparable accumulation [23]. This specific enrichment pattern implies that ac4C may uniquely regulate the targeted transport of mRNA to SGs under stress conditions. In contrast, m5C modification, characterized by low abundance and limited dynamic regulation, primarily contributes to basal cellular homeostasis and appears less directly involved in rapid stress-responsive regulation compared to ac4C [49]. Furthermore, ac4C has been shown to directly enhance mRNA translational efficiency [38, 50]. Given the well-established link between SG formation and translational arrest, we hypothesize that ac4C may influence mRNA recruitment to SGs by modulating its translational status. It is noteworthy that although m6A modification has been reported to facilitate mRNA localization to SGs through interactions with YTHDF proteins, recent studies indicate that m6A plays a limited role in the recruitment of endogenous mRNAs to SGs [51–53], further underscoring the potential uniqueness of ac4C in this pathway. This discovery provides a novel perspective for understanding the dynamic regulatory mechanisms of SGs. Under stress conditions, both NAT10 protein expression and ac4C modification abundance increased significantly. However, gene knockout experiments revealed that the absence of *NAT10* does not affect SG formation, indicating that ac4C-modified RNA is a crucial component of SGs but not an essential factor for their formation.

To further explore the biological functions of mRNA acetylation in SG, we performed acRIP-seq and RNA-seq analyses, which elucidated the roles of ac4C-modified mRNAs in SG biology. Under stress conditions, genes associated with DNA damage repair—such as ATF3, RNF168, and LIG1—exhibit significantly elevated levels of high ac4C modification. This finding suggests that ac4C

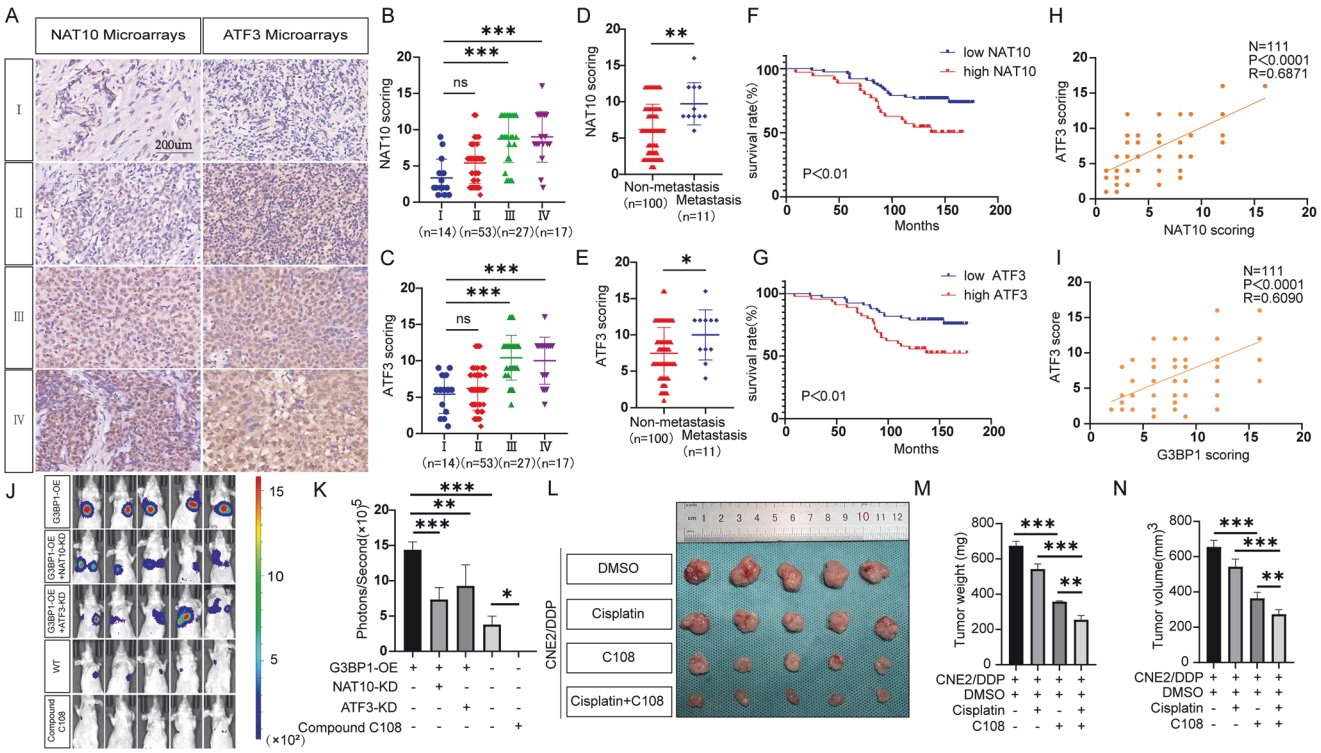

Fig. 6 The *G3BP1/NAT10/ATF3* axis is highly expressed in NPC tissues and positively correlates with disease progression. A Representative IHC staining of NAT10 and ATF3 in NPC tissue chips ($n = 111$, scale bar, 200 μm). **B**–**G** Statistical analysis of the correlation between both NAT10 and ATF3 expression levels and clinical stage, metastasis, and survival duration, respectively. **H**, **I** Correlation between ATF3 and NAT10, and ATF3 and G3BP1 levels in NPC tissues. **J** Mice were injected via the tail vein with cells overexpressing G3BP1 (CNE2-luc cells), cells overexpressing G3BP1 with ATF3 knockout, cells overexpressing G3BP1 with NAT10 knockout, CNE2-luc cells treated with Compound C108, and CNE2-luc cells. Lung metastasis visualization represents five independent experiments. **K** Average fluorescence intensity. Data are expressed as mean ± standard deviation. **L** Macroscopic images of NPC xenograft tumors. **M**–**N** Analysis of the weight and volume of NPC-derived xenograft tumors across different experimental groups (one-way ANOVA). $^*P < 0.05$, $^{**}P < 0.01$, $^{***}P < 0.001$.

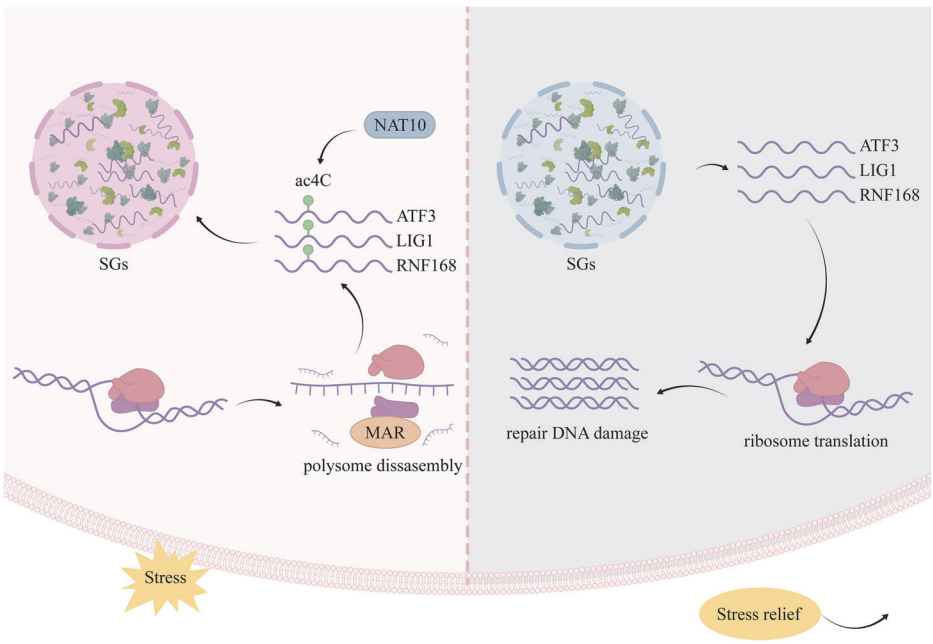

Fig. 7 Schematic diagram showing how NPC enhances survival capacity by recruiting ac4C-modified DNA damage repair genes into SGs. Left panel: Under stress, translation stalls at ribosomes. At this stage, ac4C-modified DNA damage repair genes are preferentially recruited into SGs for protection. Right panel: Upon stress resolution, these protected genes are released from SGs to repair accumulated DNA damage, thereby promoting NPC cell survival.

modification may play a key role in cellular stress responses by regulating the stability or translation efficiency of specific mRNAs. In fact, our further research revealed that under stress conditions, ac4C modification mediates the localization of DNA damage repair-related mRNAs such as ATF3, RNF168, and LIG1 to SGs, thereby achieving selective protection of these mRNAs. Interestingly, this colocalization exhibits dynamic reversible characteristics. We propose that upon stress relief, the release of these mRNAs from SGs and subsequent reactivation of their translation serves to boost DNA damage repair mechanisms, ultimately leading to a reduction in DNA damage. This discovery not only reveals a novel mechanism by which RNA modifications regulate gene expression through spatial localization but also lays the groundwork for understanding the subcellular compartmentalization functions within the epigenome. Notably, severe DNA damage persisted after stress relief in cells treated with OUL232, Compound C108, or *NAT10* knockout. This suggests that the synergistic effect between MARylation and NAT10 underscores the significance of cross-talk between protein post-translational modifications and RNA modifications in regulating SG function. Specifically, MARylation maintains the structural integrity of SG, while ac4C ensures the precise recruitment of DDR mRNA. Together, they form the molecular basis for cellular stress adaptation.

Our study establishes the *G3BP1/NAT10/ATF3* axis as a key driver of NPC progression. Clinically, its overexpression is significantly correlated with advanced clinical stage (IV), distant metastasis, lymph node metastasis, and unfavorable overall survival in NPC patients. Mechanistically, we demonstrated that G3BP1 fosters NPC tumor growth both in vitro and in vivo. Notably, inhibition of SG assembly effectively restores cisplatin sensitivity in tumor models, underscoring its dual function in promoting malignant progression and conferring chemoresistance. Taken together, these findings establish the *G3BP1/NAT10/ATF3* axis not only as a potent oncogenic pathway in NPC but also as a promising therapeutic target for overcoming cisplatin resistance.

DATA AVAILABILITY

All data generated or analyzed during this study are included in this article and its Supplementary Information Files.

REFERENCES

1. Chen YP, Chan ATC, Le QT, Blanchard P, Sun Y, Ma J. Nasopharyngeal carcinoma. Lancet. 2019;394:64–80.
2. Chen S, Yang D, Liao X, Lu Y, Yu B, Xu M, et al. Failure patterns of recurrence and metastasis after intensity-modulated radiotherapy in patients with nasopharyngeal carcinoma: results of a multicentric clinical study. Front Oncol. 2022;11:693199.
3. Wang H. Metabolic reprogramming in the pathogenesis and progression of nasopharyngeal carcinoma: molecular mechanisms and therapeutic implications. Am J Cancer Res. 2024;14:4049–64.
4. Labrie M, Brugge JS, Mills GB, Zervantonakis IK. Therapy resistance: opportunities created by adaptive responses to targeted therapies in cancer. Nat Rev Cancer. 2022;22:323–39.
5. Chen X, Cubillos-Ruiz JR. Endoplasmic reticulum stress signals in the tumour and its microenvironment. Nat Rev Cancer. 2021;21:71–88.
6. Grabocka E, Bar-Sagi D. Mutant KRAS enhances tumor cell fitness by upregulating stress granules. Cell. 2016;167:1803–13.e12.
7. Millar SR, Huang JQ, Schreiber KJ, Tsai YC, Won J, Zhang J, et al. A new phase of networking: the molecular composition and regulatory dynamics of mammalian stress granules. Chem Rev. 2023;123:9036–64.
8. Song D, Kuang L, Yang L, Wang L, Li H, Li X, et al. Yin and yang regulation of stress granules by Caprin-1. Proc Natl Acad Sci USA. 2022;119:e2207975119.
9. Yang P, Mathieu C, Kolaitis RM, Zhang P, Messing J, Yurtsever U, et al. G3BP1 is a tunable switch that triggers phase separation to assemble stress granules. Cell. 2020;181:325–45.e28.
10. Chatterjee D, Chakrabarti O. Role of stress granules in modulating senescence and promoting cancer progression: special emphasis on glioma. Int J Cancer. 2022;150:551–61.
11. Dudman J, Qi X. Stress granule dysregulation in amyotrophic lateral sclerosis. Front Cell Neurosci. 2020;14:598517.
12. Mahboubi H, Stochaj U. Cytoplasmic stress granules: dynamic modulators of cell signaling and disease. Biochim Biophys Acta Mol Basis Dis. 2017;1863:884–95.
13. Wang Z, Zhang C, Fan C, Liu Y. Post-translational modifications in stress granule and their implications in neurodegenerative diseases. Biochim Biophys Acta Gene Regul Mechan. 2023;1866:194989.
14. Mateju D, Eichenberger B, Voigt F, Eglinger J, Roth G, Chao JA. Single-molecule imaging reveals translation of mRNAs localized to stress granules. Cell. 2020;183:1801–12.e13.
15. Bley N, Lederer M, Pfalz B, Reinke C, Fuchs T, Glaß M, et al. Stress granules are dispensable for mRNA stabilization during cellular stress. Nucleic Acids Res. 2015;43:e26.
16. Protter DSW, Parker R. Principles and properties of stress granules. Trends Cell Biol. 2016;26:668–79.
17. Dai H, Wang G, Cao W, Qi W, Chen W, Guo H. Stress granules affect the sensitivity of renal cancer cells to sorafenib by sequestering and stabilizing COX-2 mRNA. Oncol Lett. 2023;25:274.
18. Thedieck K, Holzwarth B, Prentzell MT, Boehlke C, Kläsener K, Ruf S, et al. Inhibition of mTORC1 by astrin and stress granules prevents apoptosis in cancer cells. Cell. 2013;154:859–74.
19. Roundtree IA, Evans ME, Pan T, He C. Dynamic RNA modifications in gene expression regulation. Cell. 2017;169:1187–200.
20. Cui L, Ma R, Cai J, Guo C, Chen Z, Yao L, et al. RNA modifications: importance in immune cell biology and related diseases. Sig Transduct Target Ther. 2022;7:334.
21. Qiu L, Jing Q, Li Y, Han J. RNA modification: mechanisms and therapeutic targets. Mol Biomed. 2023;4:25.
22. Xie L, Zhong X, Cao W, Liu J, Zu X, Chen L. Mechanisms of NAT10 as ac4C writer in diseases. Mol Ther Nucleic Acids. 2023;32:359–68.
23. Kudrin P, Singh A, Meierhofer D, Kuśnierczyk A, Ørom UAV. N4-acetylcytidine (ac4C) promotes mRNA localization to stress granules. EMBO Rep. 2024;25:1814–34.
24. Yang Q, Lei X, He J, Peng Y, Zhang Y, Ling R, et al. N4-acetylcytidine drives glycolysis addiction in gastric cancer via NAT10/SEPT9/HIF-1 *α* positive feedback loop. Adv Sci. 2023;10:2300898.
25. Bao L, You B, Shi S, Shan Y, Zhang Q, Yue H, et al. Metastasis-associated miR-23a from nasopharyngeal carcinoma-derived exosomes mediates angiogenesis by repressing a novel target gene TSGA10. Oncogene. 2018;37:2873–89.
26. Khong A, Matheny T, Jain S, Mitchell SF, Wheeler JR, Parker R. The stress granule transcriptome reveals principles of mRNA accumulation in stress granules. Mol Cell. 2017;68:808–20.e5.
27. Khong A, Jain S, Matheny T, Wheeler JR, Parker R. Isolation of mammalian stress granule cores for RNA-Seq analysis. Methods. 2018;137:49–54.
28. Aguilera-Gomez A, Van Oorschot MM, Veenendaal T, Rabouille C. In vivo vizualisation of mono-ADP-ribosylation by dPARP16 upon amino-acid starvation. eLife. 2016;5:e21475.
29. Hottiger MO, Hassa PO, Lüscher B, Schüler H, Koch-Nolte F. Toward a unified nomenclature for mammalian ADP-ribosyltransferases. Trends Biochem Sci. 2010;35:208–19.
30. Longarini EJ, Dauben H, Locatelli C, Wondisford AR, Smith R, Muench C, et al. Modular antibodies reveal DNA damage-induced mono-ADP-ribosylation as a second wave of PARP1 signaling. Mol Cell. 2023;83:1743–60.e11.
31. Lüscher B, Bütepage M, Eckei L, Krieg S, Verheugd P, Shilton BH. ADP-ribosylation, a multifaceted posttranslational modification involved in the control of cell physiology in health and disease. Chem Rev. 2018;118:1092–136.
32. Cohen MS, Chang P. Insights into the biogenesis, function, and regulation of ADP-ribosylation. Nat Chem Biol. 2018;14:236–43.
33. Daugherty MD, Young JM, Kerns JA, Malik HS. Rapid evolution of PARP genes suggests a broad role for ADP-ribosylation in host-virus conflicts. PLoS Genet. 2014;10:e1004403.
34. Leung AKL. Poly(ADP-ribose): a dynamic trigger for biomolecular condensate formation. Trends Cell Biol. 2020;30:370–83.
35. Jayabalan AK, Bhambhani K, Leung AK. PARP10 is critical for stress granule initiation. Life Sci Alliance. 2025;8:e202403026.
36. Murthy S, Nizi MG, Maksimainen MM, Massari S, Alaviuhkola J, Lippok BE, et al. [1,2,4]Triazolo[3,4- *b*]benzothiazole scaffold as versatile nicotinamide mimic allowing nanomolar inhibition of different PARP enzymes. J Med Chem. 2023;66:1301–20.
37. Gupta N, Badeaux M, Liu Y, Naxerova K, Sgroi D, Munn LL, et al. Stress granule-associated protein G3BP2 regulates breast tumor initiation. Proc Natl Acad Sci USA 2017;114:1033–8.
38. Arango D, Sturgill D, Yang R, Kanai T, Bauer P, Roy J, et al. Direct epitranscriptomic regulation of mammalian translation initiation through N4-acetylcytidine. Mol Cell. 2022;82:2797–814.e11.
39. Ma N, Liu H, Wu Y, Yao M, Zhang B. Inhibition of N-acetyltransferase 10 suppresses the progression of prostate cancer through regulation of DNA replication. IJMS. 2022;23:6573.

40. Buchan JR, Parker R. Eukaryotic stress granules: the ins and out of translation. Mol Cell. 2009;36:932.
41. Cao X, Jin X, Liu B. The involvement of stress granules in aging and aging-associated diseases. Aging Cell. 2020;19:e13136.
42. Fu Y, Zhuang X. m6A-binding YTHDF proteins promote stress granule formation. Nat Chem Biol. 2020;16:955–63.
43. Ries RJ, Zaccara S, Klein P, Olarerin-George A, Namkoong S, Pickering BF, et al. m6A enhances the phase separation potential of mRNA. Nature. 2019;571:424–8.
44. Grimaldi G, Catara G, Palazzo L, Corteggio A, Valente C, Corda D. PARPs and PAR as novel pharmacological targets for the treatment of stress granule-associated disorders. Biochem Pharmacol. 2019;167:64–75.
45. Zhong S, Yin H. Stress granules shape metabolic reprogramming and drug resistance. Nat Cancer. 2025;6:1129–30.
46. Jia Y, Jia R, Dai Z, Zhou J, Ruan J, Chng W, et al. Stress granules in cancer: adaptive dynamics and therapeutic implications. iScience. 2024;27:110359.
47. Challa S, Khulpateea BR, Nandu T, Camacho CV, Ryu KW, Chen H, et al. Ribosome ADP-ribosylation inhibits translation and maintains proteostasis in cancers. Cell. 2021;184:4531–46.e26.
48. Challa S, Nandu T, Kim HB, Gong X, Renshaw CW, Li WC, et al. RACK1 MARylation regulates translation and stress granules in ovarian cancer cells. J Cell Biol. 2025;224:e202401101.
49. Wang R, Ding L, Lin Y, Luo W, Xu Z, Li W, et al. The quiet giant: identification, effectors, molecular mechanism, physiological and pathological function in mRNA 5-methylcytosine modification. Int J Biol Sci. 2024;20:6241–54.
50. Arango D, Sturgill D, Alhusaini N, Dillman AA, Sweet TJ, Hanson G, et al. Acetylation of cytidine in mRNA promotes translation efficiency. Cell. 2018;175:1872–86.e24.
51. Anders M, Chelysheva I, Goebel I, Trenkner T, Zhou J, Mao Y, et al. Dynamic m^6A methylation facilitates mRNA triaging to stress granules. Life Sci Alliance. 2018;1:e201800113.
52. Khong A, Matheny T, Huynh TN, Babl V, Parker R. Limited effects of m6A modification on mRNA partitioning into stress granules. Nat Commun. 2022;13:3735.
53. Ries RJ, Pickering BF, Poh HX, Namkoong S, Jaffrey SR. m6A governs length-dependent enrichment of mRNAs in stress granules. Nat Struct Mol Biol. 2023;30:1525–35.

ACKNOWLEDGEMENTS

We would like to thank the laboratory of the Institute of Otolaryngology Head and Neck Surgery, Affiliated Hospital of Nantong University, for their discussion and support.

AUTHOR CONTRIBUTIONS

JSL and KWZ conceptualized the study; TY, HMY, LY, and JSL conceived the methodology and led the study design; TY, HMY, LY, XCX, HJX, MFG, XX, CXS, KWZ, and JSL performed the experiments; TY and HMY wrote the manuscript; and TY and HMY performed statistical analysis.

FUNDING

J Liu was supported by National Natural Science Foundation of China (grant nos. 82472772, and 82171159). T Yue, H Yin, L Yuan, X Xie, H Xie, M Gong, X Xu, C Sun and K Zhang declare no relevant funding.

COMPETING INTERESTS

The authors declare no competing interests.

ETHICS APPROVAL AND CONSENT TO PARTICIPATE

Approval for the use of patient samples was granted by the Committee for Ethical Review of Research at the Affiliated Hospital of Nantong University (Ethics Approval Number: 2019-L063). All samples were collected with informed consent. All methods were performed in accordance with the relevant guidelines and regulations. All animal experiments were conducted in accordance with the guidelines of the Nantong University Laboratory Animal Center and were approved by the Jiangsu Provincial Laboratory Animal Management Committee (Approval No: SYXK(SU)2007-0021).

ADDITIONAL INFORMATION

Supplementary information The online version contains supplementary material available at https://doi.org/10.1038/s41388-026-03792-y.

Correspondence and requests for materials should be addressed to Kaiwen Zhang or Jisheng Liu.

Reprints and permission information is available at http://www.nature.com/reprints

Publisher's note Springer Nature remains neutral with regard to jurisdictional claims in published maps and institutional affiliations.